JOURNAL OF INTEGRATED OMICS
A METHODOLOGICAL JOURNAL
HTTP://WWW.JIOMICS.COM

ORIGINAL ARTICLE | DOI: 10.5584/jiomics.v1i2.36

Quantitative Proteomic Analysis of Retina in Oxygen-Induced Retinopathy Mice using iTRAQ with 2D NanoLC-nanoESI-MS/MS

Lei Zhou[1,2,a], Liu Xinling[3,a], Siew Kwan Koh[1], Li Xiaorong*[3], Roger W Beuerman*[1,2].

[1]Singapore Eye Research Institute, Singapore; [2]Department of Ophthalmology, National University of Singapore, Singapore; [3]Tianjin Medical University Eye Center, China. [a]These authors contributed equally.

Received: 01 September 2011 **Accepted:** 22 March 2011 **Available Online**: 22 March 2011

ABSTRACT

Analysis of the retina proteome during hypoxia-induced retinal neovascularization (RN) process may be helpful to elucidate pathogenesis of related diseases, such as diabetic retinopathy (DR) and retinopathy of prematurity (ROP). Retinal neovascularization was induced in 7-day old, C57BL/6 mice by exposure to 80% oxygen for 5 days followed by 5 days in room air. Retinas from mice at postnatal day 17 from control and oxygen-induced retinopathy (OIR) groups were used for proteomic analysis. We have employed a quantitative proteomic approach, iTRAQ (isobaric Tagging for Relative and Absolute protein Quantification) coupled with 2D nanoLC-nanoESI-MS/MS to quantitatively compare the relative changes in the retina proteome from control and OIR mice. In total, 264 protein groups were identified at a 95% confidence level. Among them, OIR induced significant changes in 28 proteins (14 up-regulated and 14 down-regulated). Obvious changes include the up-regulation of a few plasma proteins (i.e. serum albumin, hemoglobin), indicating the breakdown of the blood-retina barrier. Vimentin, ribosomal proteins, some proteases, neural cell adhesion molecule (NCAM) 180, retinoschisin were found to be up-regulated and several crystallins such as isoform 1 of α crystallin A chain, isoform 2 of α crystallin A chain, α crystallin B chain, γ crystallin D and β-A3/A1 crystallin were down-regulated. The iTRAQ result of α crystallin B chain was also verified by Western blot analysis. The proteomic results from this study provide new avenues for understanding the pathogenesis of OIR induced retinal neovascularization and related retina diseases.

Keywords: Retina neovascularization; Oxygen-induced retinopathy; Retina proteome; iTRAQ; 2D nano LC-nanoESI-MS/MS.

Abbreviations

iTRAQ: isobaric tagging for Relative and Absolute protein Quantification; **OIR:** oxygen-induced retinopathy; **ROP:** retinopathy of prematurity; **VEGF:** vascular endothelial growth factor; **SCX:** strong cation exchange column; **PBS:** phosphate buffered saline; **MS/MS:** tandem mass spectrometry; **GO:** gene ontology; **FITC:** fluorescein isothiocyanate; **ESI:** electroSpray Ionization; **2D nano LC:** two-dimensional nano-liquid chromatography; **RN:** retinal neovascularization.

1. Introduction

Retina neovascularization is the hallmark of proliferative retinopathies, such as diabetic retinopathy (DR), retinopathy of prematurity (ROP), central and branch retina vein occlusion (CRVO and BRVO), all of which constitute primary causes of blindness. Inappropriate proliferation of vessels derived from preexisting retinal vessels results from hypoxic conditions including non-perfusion of the retina or a decrease in oxygen tension, which may lead to more serious complications, such as vitreous hemorrhage, tractional retinal detachment, and pre-retinal membrane formation [1, 2].

Because of the difficulty of obtaining human retina samples, an animal model of retina neovascularization is of criti-

***Corresponding author:** Prof. Roger W Beuerman, Singapore Eye Research Institute, 11 Third Hospital Avenue, Singapore 168751. E-mail Address: rwbeuer@mac.com. Prof. Li Xiaorong, Tianjin Medical University Eye Center, 64 Tongan Road, Heping district,Tianjin, China 300070. Fax: +86-22-23346434. E-mail Address: xiaorli@163.com.

cal importance. The mouse model of oxygen-induced retinopathy (OIR) is widely used to induce retinal neovascularization and serves as a model of the childhood disease of retinopathy of prematurity [3,4]. Neonatal C57BL/6 mice are exposed to a constant high (75%) oxygen level from postnatal day 7 to 12. By postnatal day 17, after five days of recovery in room air, revascularization of a central avascular area is seen with associated marked retinal neovascularization at the border between the central avascular and peripheral vascular retina [5]. Similar to proliferative diabetic retinopathy (PDR) and ROP, OIR is characterized by hypoxia-induced retinal neovascularization.

Retinal neovascularization is suggested to develop as result of a imbalance between angiogenic stimulators and inhibitors, which involves numerous growth factors, inhibiting factors, extracellular matrix proteins, vascular endothelial cells and pericytes [6, 7]. Vascular endothelial growth factor (VEGF), insulin-like growth factor (IGF), fibroblast growth factor (FGF), placental growth factor (PIGF), integrins, transforming growth factor (TGF), tissue factor (TF), and VE-cadherin all promote angiogenesis. On the other hand, pigment epithelium derived factor (PEDF), arrestin, endostatin, TIMPs, angiostatin may function as anti-angiogenic factors [6, 8-12]. Studies using this well-known model of angiogenesis with analysis or the retinal proteome may lead to the identification of novel drug targets for the inhibition of retina neovascularization. Blocking VEGF functions by the use of intra-vitreal injections of VEGF neutralizing antibodies, VEGF receptor antibodies, or VEGF receptor chimeric proteins have achieved clinical success [13]. Other anti-angiogenic approaches include anti-integrin, anti-IGF-1 and anti-proteinase antibodies [14] have also been considered. However, complete prevention of retinal neovascularization does not always occur. There still are many unknown features about the protein changes and the interactions of these factors in the process of RN.

In recent years, proteomics has been used to analyze the protein during the development of the mouse retina, mouse photoreceptor sensory cilium complex and a mouse model of retinal photoreceptor degeneration [15-17]. Additional studies have begun to examine the proteomic analysis of various retina diseases, such as age-related degeneration, diabetic retinopathy and retinal degeneration using rat or human samples [18-21]. However, there is no report on the differential proteomic analysis of mouse OIR.

In this paper, we describe the quantitative proteomic analysis of the mouse retina after varying oxygen tension to induce retinal neovascularization to retinas from normal mice using 2D nanoLC-nanoESI-MS/MS combined with iTRAQ (isobaric Tagging for Relative and Absolute protein Quantification). We have uncovered novel proteins, which may have mechanistic significance for understanding retinal neovascularization.

2. Materials and methods

Rodent Model of ROP

All experimental procedures and use of animals followed the protocol approved by the Tianjin Medical University Animal Research Committee and were in accordance with the ARVO (The Association for Research in Vision and Ophthalmology) Statement for the Use of Animals in Ophthalmic and Vision Research.

Forty female C57BL/6 mice were provided by the Experimental Animal Center of the Chinese Science Academe. Mothers and pups received standard laboratory diet and water ad libitum. Light was cycled on a 12-hour-on, 12-hour -off, and the room was maintained at approximately 21°C. Oxygen-induced retinopathy was developed in mice pups according to a protocol previously established for the mouse model of ROP [5]. In brief, at postnatal day 7, mice pups and their nursing mothers were exposed to hyperoxic conditions (80% oxygen) for 5 days in an infant incubator. On postnatal day 12, the pups were returned to room-air (normoxic conditions) for 5 days until postnatal day 17. Control groups were age-matched animals maintained in room air for the duration of the experiment.

Neo-vascularization onset and severity were measured in retinas using fluorescein-labeled dextran (2×10^6 average MW; Sigma, USA) staining. At the conclusion of the experiments, animals were anesthetized and the right atrium used as the route to perfuse the right ventricle with 1 ml phosphate-buffered saline containing 50 mg/mL fluorescein-labeled dextran. After fixing for 1 hour in 10% phosphate-buffered formalin, the entire retina was carefully dissected from the posterior eye cup, radially cut from the edge of the retina to the equator in all four quadrants. Histology was carried out to determine the presence of neovascularlization, briefly, 20 hematoxylin and eosin–stained serial sections (ten on each side of the optic nerve) per eye, at an interval of 20 μm, were examined in masked fashion for the presence of neovascular buds projecting into the vitreous from the retina. In total 34 eyes from both control group (17 eyes) and OIR group (17 eyes) were assessed using a retinal scoring system [22]. In that scoring system, blood vessel growth, blood vessel tufts, extra retinal neovascularization, central vasoconstriction, retinal hemorrhage, and tortuosity of the blood vessels were scored (0 to 4) according to certain criteria [22]. The neovascular score was defined as the mean number of neovascular tufts per section. The mean scores and standard deviations (SDs) for the control and OIR groups were calculated and statistical analysis (student t-test) was performed to determine the group differences.

Extraction of retinal protein

At postnatal day 17, 40 mice including 20 OIR treated mice and 20 age-matched control mice were sacrificed by cervical dislocation. Retinas were separated from retinal pigment epithelium (RPE), after which 1.5 times the volume of

lysis buffer was added (20% Sucrose, Tris acetate 20mM, $MgCl_2$ 2mM, Glucose 10mM, 2% CHAPS, pH7.2). Samples were homogenized at 4°C for 30 min and centrifuged for 10 min at 6,000 g and the supernatant was kept. Total protein concentration was measured on a Model 550 Microplate Reader using a Micro BCA™ Protein Assay Kit (Pierce, USA).

iTRAQ labeling of retina proteins

For quantitative proteomic analysis, 20 OIR retinal samples were pooled to form OIR group and 20 control retinal samples were pooled to form the control group.

Briefly, 50μg total protein from both control and OIR groups were digested in parallel with trypsin and then labeled with one of the four-iTRAQ reagents following the manufacturer's instructions (Applied Biosystems, Foster City, CA), in the following manner: 114 and 115 reagent for age-matched control (duplicated), 116 and 117 for OIR (duplicated). After labeling with iTRAQ, these four samples were combined (a total of 200μg protein) and subjected to 2D nanoLC-nanoESI-MS/MS (Dionex, Sunnyvale, CA and Applied Biosystems, Foster City, CA) analysis.

Proteomic analysis by 2D nanoLC-nano-ESI-MS/MS

Two-dimensional nanoLC-nanoESI-MS/MS was used for the analysis. The first dimension was a SCX column (300 mm i.d. x 10 cm porosity 10S SCX, Dionex) with 10 steps of salt plug (20μl injection) elutions (10mM, 20 mM, 30 mM, 40 mM, 50 mM, 75 mM, 100mM, 250mM, 500mM and 1000mM ammonium acetate) all at a flow rate of 30μl/min and using a loading solvent of 0.1% formic acid/ACN (95:5, v:v). The second dimension was RP separation. The 10 cm × 75 μm i.d. microcapillary LC column was self-packed using PicoFrit (New Objectives, Woburn, MA). This column had an integrated spray tip which was directly coupled with the nano-spray interface (Protana, Odense, Denmark) into Applied Biosystems' QSTAR mass spectrometer. The packing material was Luna C18, 3μm, 100 Å (Phenomenex Torrance, CA). Samples were loaded onto a trapping cartridge (C18, 0.3 x 5 mm, from Dionex) from Famos autosampler (Dionex) at 30 μL/min. After a 5 min wash with acetonitrile/water (2/98, v/v with 0.1% formic acid), the system was switched (Switchos, Dionex) into line with the C18 analytical capillary column. Using an Ultimate solvent delivery system (Dionex), a linear gradient of acetonitrile (0.1% formic acid) from 20% to 95% over 85 min at flow rate of 300 nL/min was used to analyze Parameters for the nanospray and other instrumentation were set as follows: ionspray voltage (IS) = 2200 V, curtain gas (CUR) = 20, declustering potential (DP) = 60 V, focusing potential (FP) = 265 V, collision gas setting (CAD) = 5 for nitrogen gas, DP2=15. All data was acquired using information-dependent acquisition (IDA) mode with Analyst QS software (Applied Biosystems). TOF-MS survey scan parameters were set as follows: 1 sec TOF MS survery scan in the mass range of 300~1200 Da followed by two product ion scans of 3 sec each in the mass range of 100~1500 Da. The "enhance all" function was used in the IDA experiments. Switching criteria were set to ions greater than m/z = 350 and smaller than m/z = 1200 with charge state of 2 to 4 and an abundance threshold of > 20 counts/s. Former target ions were excluded for 60s. IDA collision energy (CE) parameter script was used for automatically controlling the CE.

Database searching

The data output from the MS/MS was processed and searched against the International Protein Index (IPI, Version 3.01) protein database, under mouse taxonomy, using ProteinPilot™ software (Applied Biosystems, Foster City, CA). All protein identification was based on the criteria of Unused ProtScore > 1.3 (95% confidence). The Unused ProtScore is a measurement of all the peptide evidence for a protein that is not better explained by a higher-ranking protein. It is the true indicator of protein confidence. Protein quantitation was also carried out using ProteinPilot software (Applied Biosystems). Protein quantitation was achieved by averaging iTRAQ ratios of all peptides identified; normalization, using a Gaussian distribution with median of 1 when all peptides were considered between control and experimental groups, was performed after iTRAQ ratios were calculated.

Western Blot

Protein concentration was determined using BCA method with bovine serum albumin as standard. Protein samples (20 μg of total protein for each sample) were subjected to sodium dodecyl sulfate – polyacrylamide gel electrophoresis (SDS-PAGE) using 15% SDS – polyacrylamide gels, followed by electrophoretic blotting (overnight at 0.02A) onto nitrocellulose membranes. The blots were blocked with 5% skim milk in Tris-buffered saline – 0.2% Tween 20 for 1 hr. The blots were probed with primary polyclonal antibodies against α crystallin B chain (using dilution of 1:500), for 3 mouse control retina samples and 3 mouse OIR retina samples for 3 hrs. It was followed by incubation with the corresponding horseradish peroxidase-conjugated secondary antibodies (using dilution of 1:10000). Actin protein expression was detected on the same membranes as a loading control. Specific protein bands were detected with Immobilon Western Chemiluminescent HRP Substrate (Millipore) using the enhanced chemiluminescence western blot analysis system (Bio-Rad, USA). The membrane was exposed to x-ray films and developed (Fujifilm).

3. Results

Retina Histopathology

Representative retinal fluorescein-labeled dextran stained

flatmounts are illustrated in Figure 1A. At postnatal day 17, the OIR group exhibited the characteristics central hypoperfusion area with neovascular tufts extending into the vitreous which were not seen when compared with age-matched controls (Fig. 1B). In paraffin cross-sections of OIR treated mouse retinas, large clusters of blood vessels were adherent to the internal limiting membrane (ILM), and many blood vessels were observed in the inner retina. In some cases, retinal hemorrhage in the peripheral retina was also noticeable (Fig. 1C and 1D). The neovascular scores for control group and OIR group at postnatal day 17 were 0.23 ± 0.18 and 28.24 ± 2.51 ($p<0.001$).

Mouse retina proteome

In total 2912 distinct peptides (peptide confidence level: 95%) were identified which matched 1041 proteins before grouping. After grouping, 264 protein groups in mouse retina were identified from the iTRAQ experiments (Table 1 – Supplementary File). The threshold we used for identification of proteins was 95% confidence (or unused ProtScore > 1.3) in ProteinPilot software. Sequence coverage (%) and number of unique peptides for each protein group are also listed in the Table 1. Of the 261 proteins with quantitative information, 218 proteins have more than one peptide contributing to the quantitative results. In many cases, same peptide fragment could be acquired repeatedly by mass spectrometer and contributed to the average protein ratio.

Gene ontology (GO) annotations were analyzed using online tools, CateGOrizer [23]. Based on the GO classification, among these 264 proteins, there are 209 proteins which have at least one identifier under "biological process" (Figure 2). Genes representing other functional groups of identified proteins belonged to cell metabolism (35.6%, n=94), cellular process (30.0%, n=80), development (11.4%, n=30) and neuronal/visual (8.0%, n=21) respectively. Some proteins had

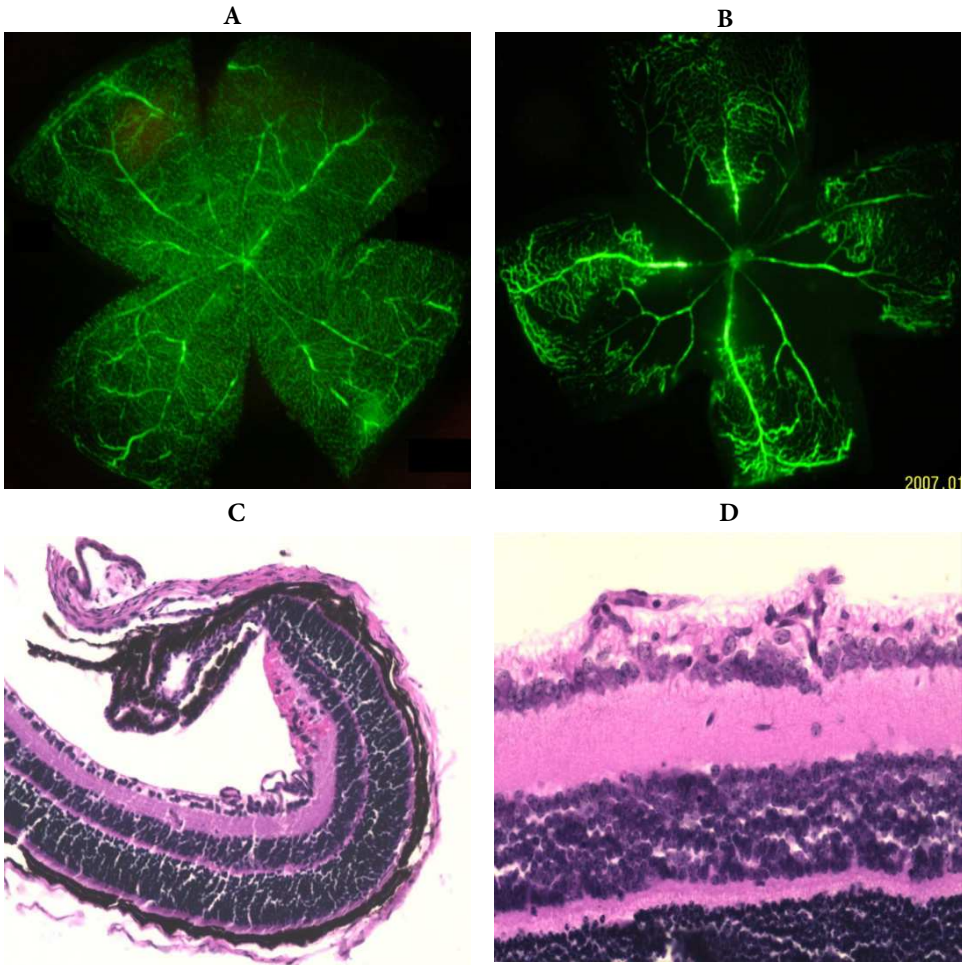

Figure 1. Fluorescein-dextran perfused retinas of mice exposed to room air or hyperoxia. (A) the retina from P17 room air-raised mouse showing the normal pattern of retina vessels. (B) retina from P17 mouse exposed to 80% oxygen from P7 to P12. (C) and (D) 10 μm paraffin cross-sections of C57BL/6 mice retinas stained with PAS and hematoxylin. Arrows indicate neovascular tufts extending into the vitreous. Retinal hemorrhage in the peripheral retina. V vitreous; ILM internal limiting membrane; GCL, ganglion cell layer; IPL inner plexiform layer.

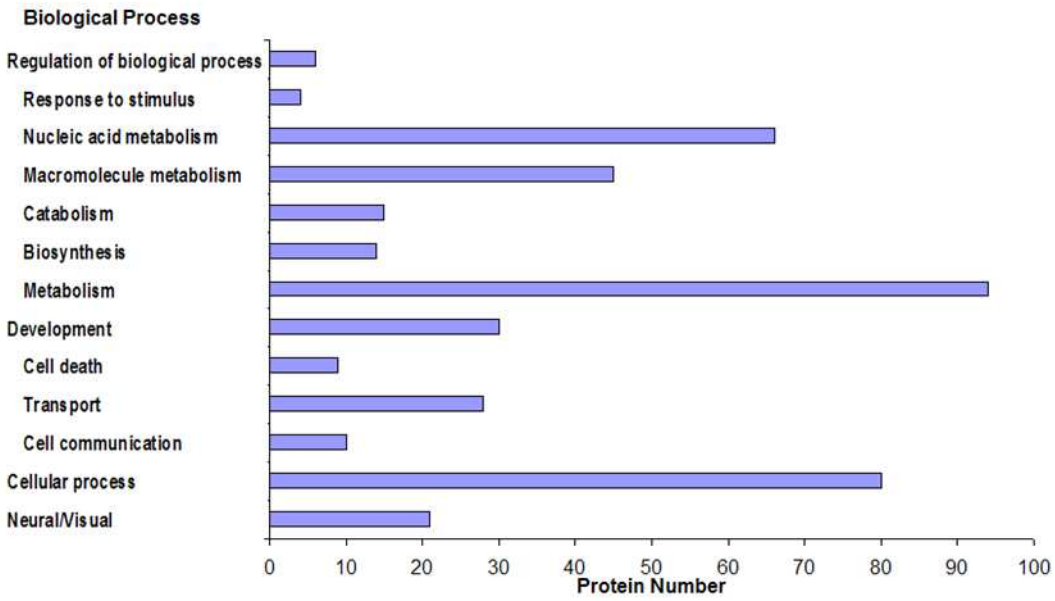

Figure 2. Gene Ontology (GO) annotation under "biological process". X-axis represents the number of proteins under each subcategory.

more than one GO identifier.

Protein profile changes in OIR mice retina

Relative quantification of the identified peptides was based on the individual ratios from signature ion (m/z = 114, 115, 116, or 117) peak areas of the iTRAQ reagent tags of the identified peptides from OIR samples compared with those of the age-matched control group. The iTRAQ ratios of all peptides for each protein were grouped, averaged and were expressed as ratios at the protein level. In this study, control and OIR groups were duplicated, i.e. iTRAQ reagents 114 and 115 were used to label two duplicated control samples and iTRAQ reagents 116 and 117were used to label two duplicated OIR samples. If we used a 20% increase or decrease for iTRAQ ratios as the cutoff, the levels of 14 proteins were found to be increased in OIR group and the levels of 14 proteins decreased in OIR group. The list of proteins found to be increased or decreased by 20% between the OIR and control groups is seen in Table 2. Figure 3 shows two representative MS/MS spectra of peptide fragments originating from vimentin (IPI00227299.5) and α crystallin B (IPI00138274.1), and relative quantitation in the mass range for the reporter ions (m/z = 114, 115, 116, or 117).

Verification by Western Blot Analysis

One of the proteins, α crystallin B chain, showed significant down-regulated in OIR group as indicated by iTRAQ was subsequently verified using Western blot analysis. Figure 4 shows Western blot results of 3 control and 3 OIR retina samples. Compared with control retina samples, the levels of α crystallin B chain were significantly decreased in OIR treated retina samples.

4. Discussion

The aim of this study was to obtain a mouse retinal proteome that responded to changes in oxygen tension causing pathological neo-vascularization. Previous studies [24] and our study shows that neovascularization was most prominent at P17. Thus, we used P17 tissues from both normal and OIR mice for the quantitative proteomic analysis. Pooled sample were used in this study for several reasons, including reducing biological variation, saving analysis time and cost, better suitability for small tissue size and sample volume. However, the information for individual biological variation is missing.

We have identified 264 protein groups (Unused ProtScore >1.3, 95% confidence) in P17 normal and OIR mice retina using 2D nanoLC-nanoESI-MS/MS. Gene ontology (GO) classification showed that the three largest functional categories are related to metabolism, cellular process and development. Twenty-one proteins are associated with neuronal/visual (8%). Among these 264 identified proteins, the levels of 14 proteins were found to be at least 20% higher in the OIR group when compared to the control group, whereas, the levels of 14 other proteins were at least 20% lower in the OIR group compared to the control group.

Proteins increased in OIR

As expected, some plasma proteins including hemoglobin and serum albumin are significantly increased in the OIR retina which may be due to breakdown of the blood-retinal barrier or an increase in leaky retinal capillaries. Retinal hemorrhage was observed in the peripheral retina of OIR mice (Fig.1c), which can directly increase the content of blood constituent proteins. Other proteomic studies showed

Table 2. Differential expression of retina proteins in oxygen-induced retinopathy (OIR) compared to age-matched control group.

N	Accession #	Name	Ratio 1	Ratio 2	Avg. Ratio	Molecular function	Biological Process	Cell component
1	IPI:IPI00469114.4	Hemoglobin subunit alpha	2.215	2.126	2.170	erythrocyte development / in utero embryonic development/ oxygen transport	heme binding/ iron ion binding/ oxygen binding/ oxygen transporter activity	hemoglobin complex
2	IPI:IPI00465823.3	similar to 60S ribosomal protein L18	1.982	1.996	1.989	Structural constituent of ribosome	translation	Intracellular/ ribosome
3	IPI:IPI00122971.1	Isoform N-CAM 180 of Neural cell adhesion molecule 1, 180 kDa isoform precursor	1.407	1.432	1.420	Protein binding/ heparin binding	Cell adhesion/cell surface receptor linked signal transduction/ positive regulation of calcium-mediated signaling/ homotypic cell-cell adhesion	anchored to membrane/ integral to membrane/ external side of plasma membrane/ axon
4	IPI:IPI00775948.1	60S ribosomal protein L7	1.509	1.285	1.392	RNA binding/ structural constituent of ribosome/ transciption regulator activity	translation	Ribosome/ cytosolic large ribosomal subunit
5	IPI:IPI00131695.3	Serum albumin precursor	1.413	1.332	1.372	DNA binding /drug binding / protein binding / pyridoxal phosphate binding /toxin binding	cellular response to starvation / hemolysis by symbiont of host red blood cells / maintenance of mitochondrion localization/ negative regulation of apoptosis	cytoplasm/protein complex/
6	IPI:IPI00227299.5	Vimentin	1.378	1.361	1.370	protein binding / structural molecule activity	intermediate filament-based process	cytoplasm / type III intermediate filament
7	IPI:IPI00785308.1	Prss3 protein (Fragment)	1.272	1.360	1.315	serine-type endopeptidase activity	proteolysis	
8	IPI:IPI00676858.1	similar to 40S ribosomal protein SA	1.276	1.342	1.309			
9	IPI:IPI00404551.1	B6-derived CD11 +ve dendritic cells cDNA, RIKEN full-length enriched library, clone:F730002E02 product: cathepsin D, full insert sequence	1.348	1.239	1.293	cathepsin D activity	proteolysis	lysosome / mitochondrion
10	IPI:IPI00130252.1	Retinoschisin precursor	1.222	1.363	1.290	Protein binding	Cell adhesion	Extracellular region
11	IPI:IPI00169463.1	Tubulin beta-2C chain	1.245	1.329	1.286	GTP binding/ GTPase activity/ structural molecule activity	Microtubule-based process/ protein polymerization	tubulin complex/ protien complex/ microtubule
12	IPI:IPI00459374.3	similar to Carbonyl reductase [NADPH] 1	1.230	1.210	1.220			
13	IPI:IPI00471441.1	Ptms protein	1.215	1.204	1.210	translation initiation factor activity	translational initiation	
14	IPI:IPI00230394.4	Lamin-B1	1.209	1.201	1.205	structural molecule activity		lamin filament
15	IPI:IPI00756474.1	similar to Splicing factor, arginine/serine-rich 3	0.781	0.800	0.790			
16	IPI:IPI00626755.4	9 kDa protein	0.757	0.799	0.778	nucleus/ DNA binding		chromatin/ cytoplasm
17	IPI:IPI00123313.1	Ubiquitin-activating enzyme E1 X	0.761	0.790	0.776	ATP binding/ ligase activity/ small protein activating enzyme activity	protein modification process/ ubiquitin-dependent protein catabolic process	
18	IPI:IPI00403058.1	Isoform 1 of Neutral alpha-glucosidase AB precursor	0.779	0.7288	0.754	glucan 1,3-alpha-glucosidase activity/ protein binding	N-glycan processing	Golgi apparatus/ alpha-glucosidase II complex/ melanosome
19	IPI:IPI00415403.1	Isoform 2 of Syntaxin-binding protein 1	0.749	0.744	0.746	protein binding	Protein transport/synaptic vesicle maturation/vesicle docking during exocytosis	mitochondrion
20	IPI:IPI00776358.1	acetyl-Coenzyme A acetyltransferase 3	0.741	0.737	0.739	transferase activity	metabolic process	

21	IPI:IPI00113536.2	Anp32b protein	0.765	0.706	0.735	protein binding		nucleus
22	IPI:IPI00606097.1	transmembrane protease, serine 13	0.578	0.493	0.534	scavenger receptor activity/ serine-type endopeptidase activity	proteolysis	integral to membrane
23	IPI:IPI00113845.1	Proteasome subunit beta type 1 precursor	0.340	0.697	0.486	threonine-type endopeptidase activity	ubiquitin-dependent protein catabolic process	cytosol/ nucleus/ proteasome core complex
24	IPI:IPI00134845.1	Beta-A3/A1 crystallin protein	0.294	0.325	0.309			
25	IPI:IPI00420923.2	Gamma crystallin D	0.286	0.262	0.274		eye development	
26	IPI:IPI00138274.1	Alpha crystallin B chain	0.231	0.2451	0.238	structural constituent of eye lens	camera-type eye development /muscle development /transmembrane receptor protein tyrosine kinase signaling pathway	insoluble / fractionplasma membrane /soluble fraction /Z disc
27	IPI:IPI00108737.1	Isoform 1 of Alpha crystallin A chain	0.203	0.217	0.210			
28	IPI:IPI00109729.1	Isoform 2 of Alpha crystallin A chain	0.136	0.105	0.120		camera-type eye development/M phase specific microtubule process	Cellular component: cytoplasm /

that the vitreous body in proliferative diabetic retinopathy had higher levels of albumin, hemopexin, and IgG, IgA, complement C3, C4 and other blood constituent proteins due to the breakdown of the blood-retina barrier [25-27]. In our study, the surrounding tissues were carefully rinsed with cold saline solution to avoid the possibility of blood contamination.

Retina diseases or injury including choroidal neovascularization, diabetic retinopathy, retinal detachment (RD), and retinal trauma can trigger reactive gliosis. In such situations, the increased production of intermediate filament proteins, vimentin, and glial fibrillary acidic protein (GFAP) are often observed [28]. In this study, the increased expression of vimentin was observed (Table 2 and Figure 3).

Our results showed the levels of three ribosomal proteins (60S ribosomal protein L18, 60S ribosomal protein L7 and 40S ribosomal protein SA) increased in the OIR treated mouse retina. Ribosomal proteins are major constituents of ribosomes that catalyze protein synthesis in the cytoplasm [29]. The eukaryotic ribosome is composed of a large (60S) and a small (40S) subunit, which consists of three RNAs and 46 proteins (60S) and one RNA and 33 proteins (40S) [30]. Under normal conditions, ribosomal proteins are synthesized precisely with rRNA to produce equimolar amounts of RNA and protein. Under altered conditions, including events surrounding cellular growth and proliferation, the expression levels of ribosomal proteins are altered. The large ribosomal subunit proteins L7 and the small ribosomal subunit proteins 40S exhibit decreased expression during neuronal differentiation of human embryonic carcinoma cells [31]. Independent alterations in ribosomal protein synthesis suggest that individual ribosomal proteins may have functions beyond the simple structural makeup of the ribosome or protein synthesis. For example, L7 can function as a coregulator of nuclear receptors and has also been implicated in apoptotic pathways in cataract formation [32]. The 40S ribosomal protein and laminin receptor precursor protein are encoded by the same gene (*37LRP/p40*) [33], suggesting it has dual functions as both a cell surface receptor and a ribosomal protein. It is overexpressed on cancer cells [34].

Proteases have been increasingly recognized as important factors in the pathophysiology of proliferative retinopathy and tumors. These are involved in the proteolytic degradation of the extracellular matrix, as well as the release and activation of growth and angiogenic factors. Prss3 protein is a kind of serine proteinase (mesotrypsin), belong to S1 peptidase family, encoded by the PRSS3 gene. Some studies suggest that it evokes a transient and pronounced Ca^{2+} mobilization in both primary rat astrocytes and retinal ganglion RGC-5 cells, suggesting a physiological role in the brain [35]. Cathepsin D (CatD) acts as a lysosomal cysteine and aspartic proteinase, which are found in most mammalian cells. CatD is one of the most important lysosomal enzymes in RPE cells and can be changed by several posttranslational modifications to produce the biologically active form. It has been proposed that the high presence of inactive forms of CatD in RPE cells can accelerate RPE debris accumulation, RPE atrophy, proliferation and the accumulation of basal lamina and linear deposits associated with retina degeneration. It may play an important role in the development and progression of malignant tumors and overexpression of cathepsin D in aggressive cancers is associated with a poor prognosis [36]. Some studies indicate it has other effects which are independent of its proteolytic activity in cancer cell proliferation and tumor angiogenesis [37].

Neural cell adhesion molecule (NCAM) is a transmembrane protein which mediates cell adhesion and migration. NCAM 180 is one of three isoforms. The level of NCAM 180 isoform was reported to be elevated in astrocytes of glaucomatous optic nerve head [38]. Retinoschisin is a photoreceptor-secreted protein which mediates interactions/adhesion between photoreceptor, bipolar, and Müller cells and contributes to the maintenance of the integrity of the cytoarchitectural of the retina [39]. The mutation of retinoschisin causes a retina disease called X-linked juvenile retinoschisis, which is characterized by morphological and electrophysio-

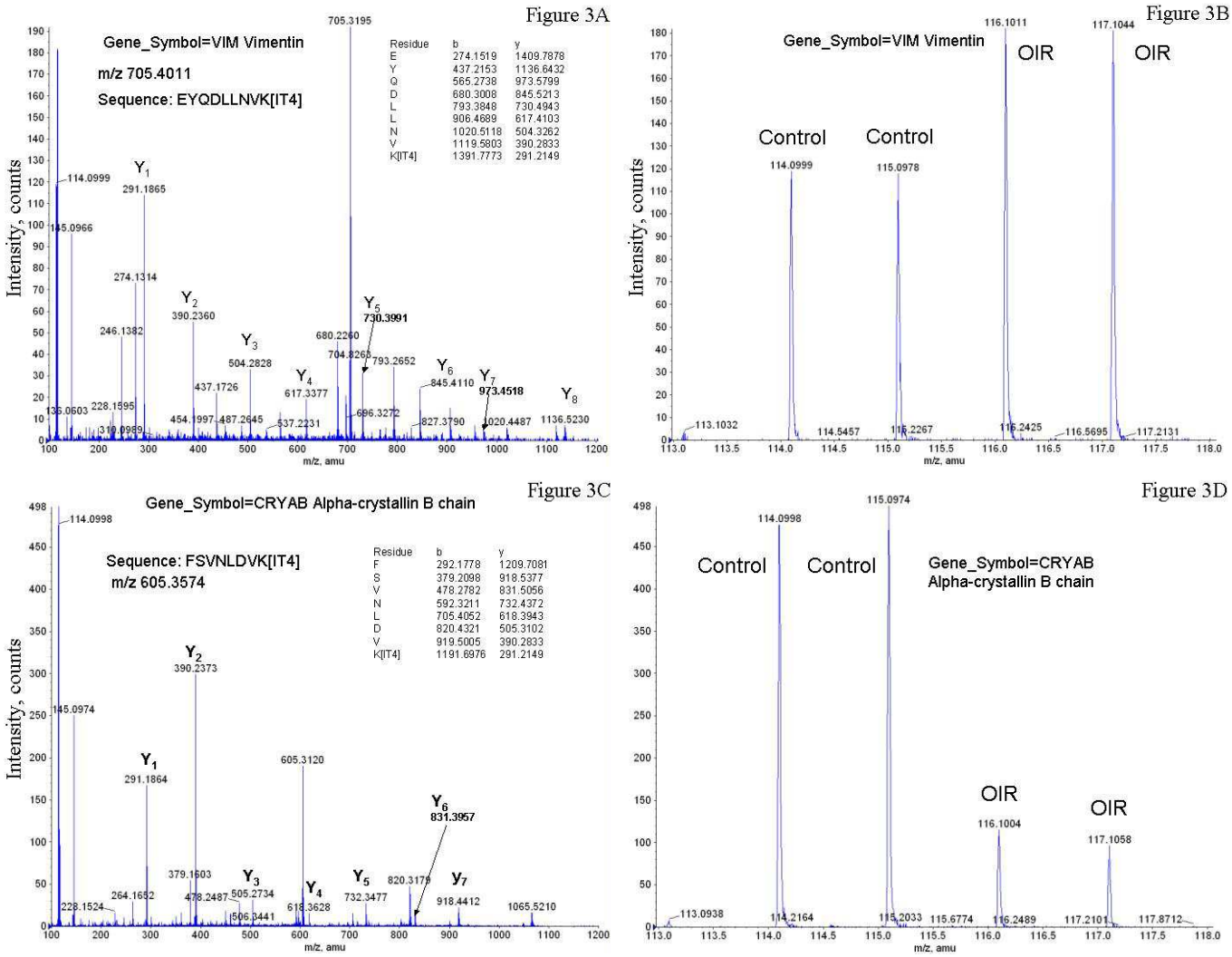

Figure 3. (A) MS/MS spectrum of one doubly charged peptide ion (EYQDLLNVK at m/z = 705.40) originated from vimentin and (B) relative quantification for vimentin between OIR samples and control samples. (C) MS/MS spectrum of one doubly charged peptide ion (FSVNLDVK at m/z = 605.36) originated from alpha-crystallin B chain. (D) relative quantification for alpha-crystallin B chain between OIR samples and control samples .

logical defects of the retina.

Proteins decreased in OIR

In this study, the crystallins were found to show the most striking changes in the retina proteome occurring between OIR treated animals and controls. We found the levels of five crystallins were down-regulated in OIR, including isoform 1 of α crystallin A chain, isoform 2 of α crystallin A chain, α crystallin B chain, γ crystallin D and β-A3/A1 crystallin. One of them, α crystallin B chain was also verified by Western blot analysis. Crystallins were originally considered to be static, abundant proteins providing transparency to the lens, and in vertebrates, three major classes of crystallins, α, β, and γ accumulate in the lens in a spatially and temporally regulated manner. Now however it is generally accepted that they also have non-lens roles and are retained in multiple tissues of the same organism [40]. Jinghua Xi [41] used microarray analysis followed by quantitative RT-PCR and found that mouse retinal cells express transcripts for 20 different members of the crystallin gene family. αA, αB, β-, and γ-crystallins are detected in the outer and inner nuclear layers, αB and β-crystallins are detected in the photoreceptor inner segments by immunoblot analysis and

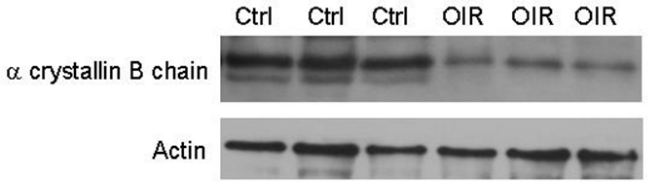

Figure 4. Western blot results of alpha-crystallin B chain in 3 mouse control retina samples and 3 mouse OIR retina samples. The bottom panel is the expression of actin used as a loading control.

immunofluorescence [42]. Several reports have identified the expression of one or more of these crystallins in the retina and showed altered crystallin transcript levels resulting from chronic elevation of intraocular pressure, diabetes, light injury, mechanical injury, and age-related macular degeneration [18, 43-46]. It has been established that α-crystallins are small heat shock proteins that act as molecular chaperones, and are distinguished from other chaperone families by their ability to prevent the non-specific aggregation of denatured proteins and their lack of ATP consumption. However, less is known about the celular functions of β/γ-crystallins. Some studies suggest that αA and αB-crystallins may be involved in fundamental processes such as genomic stability. Farjo used gene microarrays and identified many genes of the crystallin family which were significantly down-regulated in the retinas of mice with diabetic retinopathy [47] which supports an implication of our findings.

5. Conclusion

In summary, we have used 2D nanoLC-nanoESI-MS/MS combined with iTRAQ to simultaneously determine relative changes in the proteome of retina tissues obtained from OIR mice (at postnatal day 17) compared to age-matched controls. In total, 264 protein groups were identified with high confidence (ProtScore>1.3, >95% confidence). Our data suggests a series of functional changes in proteins associated with retinal angiogenesis. The results from this study may provide a basis for new insights in RN research and closer examination of these factors may ultimately generate novel therapeutic strategies of retinal diseases associated with neovascularization.

6. Supplementary material

Supplementary material regarding this manuscript is online available in the web page of JIOMICS.
http://www.jiomics.com/index.php/jio/rt/suppFiles/36/

References

1. Ray F. Gariano, Thomas W. Gardner. Retinal angiogenesis in development and disease. Nature. 2005; 438(15); 960-966.
2. Sjolie AK, Stephenson J, Aldington S, Kohner E, Janka H, et al. Retinopathy and vision loss in insulin dependent diabetes in Europe: the EURODIAB IDDM Complications Study. Ophthalmology. 1997; 104:252–260.
3. Kramerov A, Saghizadeh M, Pan H, Kabosova A, Montenarh M. Expression of protein kinase CK2 in astroglial cells of normal and neovascularized retina. Am J Pathol. 2006;168(5):1722-36.
4. Kimura T, Takagi H, Suzuma K, Kita M, Watanabe D, et al. Comparisons between the beneficial effects of different sulphonylurea treatments on ischemia-induced retinal neovascularization. Free Radic Biol Med. 2007; 43(3):454-61.
5. Smith LE, Wesolowski E, McLellan A, Kostyk SK, D'Amato R, et al. Oxygen-induced retinopathy in the mouse. Invest Ophthalmol Vis Sci, 1994, 35(1):101-111.
6. Michael Dorrell, Hannele Uusitalo-Jarvinen, Edith Aguilar, and Martin Friedlander. Ocular Neovascularization: Basic Mechanisms and Therapeutic Advances. Survey Of Ophthalmology, 2007; 52: S3--S19
7. Sarah X. Zhang, Jian-xing Ma. Ocular neovascularization: Implication of endogenous angiogenic inhibitors and potential therapy. Progress in Retinal and Eye Research 2007; 26:1–37.
8. Smith LE, Shen W, Perruzzi C, Soker S, Kinose F, et al. Regulation of vascular endothelial growth factor-dependent retinal neovascularization by insulin-like growth factor-1 receptor. Nat Med. 1999; 5:1390–1395.
9. Sarlos S, Rizkalla B, Moravski CJ, Cao Z, Cooper ME, et al. Retinal angiogenesis is mediated by an interaction between the angiotensin type2 receptor, VEGF, and angiopoietin. Am J Pathol, 2003; 163(3):879-887.
10. Dawson DW, Volpert OV, Gillis P, Crawford SE, Xu H, et al. Pigment epithelium derived factor: a potent inhibitor of angiogenesis. Science. 1999; 285:245–248.
11. Kvanta A. Ocular angiogenesis: the role of growth factors. Acta Ophthalmol Scand. 2006; 84(3):282-8.
12. Yoshida S, Yoshida A, Ishibashi T. Induction of IL-8, MCP-1, and bFGF by TNF-alpha in retinal glial cells: implications for retinal neovascularization during after ischemic inflammation. Graefes Arch Clin Exp Ophthalmol, 2004; 242:409–413.
13. Aiello, L.P., Pierce, E.A., Foley, E.D., Takagi, H., Chen, H., Riddle, L.,Ferrara, N., King, G.L., Smith, L.E.,. Suppression of retinal neovascularization in vivo by inhibition of vascular endothelial growth factor (VEGF) using soluble VEGF-receptor chimeric proteins. Proc. Natl. Acad. Sci. USA 1995 92, 10457–10461.
14. Das, A., McGuire, P.G.,. Retinal and choroidal angiogenesis: pathophysiology and strategies for inhibition. Prog. Retin. Eye Res. 2003; 22, 721–748.
15. Liu Q, Tan G, Levenkova N, Li T, Pugh EN, Rux J, Speicher DW, Pierce EA. The proteome of the mouse photoreceptor sensory cilium complex. Mol Cell Proteomics. 2007 May 9;
16. Haniu H, Komori N, Takemori N, Singh A, Ash JD, Matsumoto H. Proteomic trajectory mapping of biological transformation: Application to developmental mouse retina. Proteomics. 2006; 6(11):3251-61.
17. Cavusoglu N, Thierse D, Mohand-Saïd S, Chalmel F, Poch O, Van-Dorsselaer A, Sahel JA, Léveillard T. Differential proteomic analysis of the mouse retina: the induction of crystallin proteins by retinal degeneration in the rd1 mouse. Mol Cell Proteomics. 2003; 2(8):494-505.
18. Crabb JW, Miyagi M, Gu X, Shadrach K, West KA, et al. Drusen proteome analysis: an approach to the etiology of age related macular degeneration. Proc Natl Acad Sci, 2002; 99:14682-14687.
19. Haniu H, Komori N, Takemori N, Singh A, Ash JD,et al. Proteomic trajectory mapping of biological transformation: Application to developmental mouse retina. Proteomics. 2006; 6 (11):3251-61.
20. Godfrey J. Quin, Alice C. L. Len, Frank A. Billson, Mark C. Gillies. Proteome map of normal rat retina and comparison with the proteome of diabetic rat retina: New insight in the pathogenesis of diabetic retinopathy. 2007; 7:2636-2650.
21. Curtis L. Nordgaard, Kristin M. Berg, Rebecca J. Kapphahn, Cavan Reilly, Xiao Feng, et al. Proteomics of the Retinal Pig-

ment Epithelium Reveals Altered Protein Expression at Progressive Stages of Age-Related Macular Degeneration. Invest Ophthalmol Vis Sci, 2006, 47;3; 815-822.

22. Higgins RD, Yu K, Sanders RJ, et al. Diltiazem reduces retinal neovascularization in a mouse model of oxygen induced retinopathy. Curr Eye Res 1999; 18: 20-7
23. Zhi-Liang Hu, Jie Bao and James M. Reecy (2008) "CateGOrizer: A Web-Based Program to Batch Analyze Gene Ontology Classification Categories". Online Journal of Bioinformatics. 9 (2):108-112.
24. Sato T, Kusaka S, Hashida N, Saishin Y, Fujikado T, Tano Y. Comprehensive gene-expression profile in murine oxygen-induced retinopathy. Br J Ophthalmol. 2009 Jan;93(1):96-103.
25. Bresgen M, Baum U, Esser P, Wiedemann P, Heimann K. Protein composition of the vitreous body in proliferative diabetic retinopathy. An analysis with 2D-electrophoresis. Ophthalmologe. l994; 9l: 758—762.
26. Nakanishi T, Koyama R, Ikeda T, Shimizu A. Catalogue of soluble proteins in the human vitreous humor：comparison between diabetic retinopathy and macular hole. J Chromatogr B Analyt Technol Biomed Life Sci, 2002; 776:89-l00.
27. García-Ramírez M, Canals F, Hernández C, Colomé N, Ferrer C, et al. Proteomic analysis of human vitreous fluid by fluorescence-based difference gel electrophoresis (DIGE): a new strategy for identifying potential candidates in the pathogenesis of proliferative diabetic retinopathy. Diabetologia. 2007; 50 (6):1294-1303.
28. Nakazawa T, Takeda M, Lewis GP, Cho KS, Jiao J, Wilhelmsson U, Fisher SK, Pekny M, Chen DF, Miller JW. Attenuated glial reactions and photoreceptor degeneration after retinal detachment in mice deficient in glial fibrillary acidic protein and vimentin. Invest Ophthalmol Vis Sci. 2007 Jun;48(6):2760-8.
29. Mager WH. Control of ribosomal protein gene expression. Biochim.Biophys Acta. 1988; 949:1–15.
30. Wool IG, Chan Y-L, Gluck A. Structure and evolution of mammalian ribosomal proteins. Biochem Cell Biol. 1995; 73: 933–947.
31. Bevort M, Leffers H. Down regulation of ribosomal protein mRNAs during neuronal differentiation of human NTERA2 cells. Differentiation. 2000; 66:81–92.
32. Ben-Ishai R, Scharf R, Kapten I. A human cellular sequence implicated in trk oncogene activation is DNA damage inducible. Prod Natl Acad Sci USA. 1990;87: 6039–6043.
33. Jamieson KV, Wu J, Hubbard SR, Meruelo D. Crystal structure of the human laminin receptor precursor. J Biol Chem. 2008 Feb 8;283(6):3002-5. Epub 2007 Dec 6.
34. Mafune K, Ravikumar TS, Wong JM, et al. Expression of a Mr 32,000 laminin-binding protein messenger RNA in human colon carcinoma correlates with disease progression. Cancer Res, 1990; 50:3888–3891.
35. Yingfei Wang, Weibo Luo, Thomas Wartmann, Walter Halangk, Miklós Sahin-Tóth and Georg Reiser. Mesotrypsin, a brain trypsin, activates selectively proteinase-activated receptor -1, but not proteinase-activated receptor-2, in rat astrocytes. Journal of Neurochemistry, 2006; Volume 99 Issue 3 Page 759-769.
36. Foekens JA, Look MP, Bolt-de Vries J, Meijer-van Gelder ME, van Putten WL, et al. Cathepsin-D in primary breast cancer: prognostic evaluation involving 2810 patients. Br J Cancer. 1999 Jan;79(2):300-7.
37. Laurent-Matha V, Maruani-Herrmann S, Prébois C, Beaujouin M, Glondu M,Catalytically inactive human cathepsin D triggers fibroblast invasive growth. J Cell Biol. 2005 Jan 31;168 (3):489-99.
38. Ricard CS, Kobayashi S, Pena JD, Salvador-Silva M, Agapova O, Hernandez MR. Selective expression of neural cell adhesion molecule (NCAM)-180 in optic nerve head astrocytes exposed to elevated hydrostatic pressure in vitro. Brain Res Mol Brain Res. 2000 Sep 30;81(1-2):62-79.
39. Reid SN, Yamashita C, Farber DB. Retinoschisin, a photoreceptor-secreted protein, and its interaction with bipolar and muller cells. J Neurosci. 2003 Jul 9;23(14):6030-40.
40. Sax C, Piatigorsky J. Expression of the α-crystallin/small heat-shock protein/molecular chaperone genes in the lens and other tissues. In: Meister A, editor. Advances in enzymology and related areas of molecular biology. Vol 69. New York: Wiley Interscience; 1994:155-201.
41. Jinghua Xi, Rafal Farjo, Shigeo Yoshida, etal. A comprehensive analysis of the expression of crystallins in mouse retina. Molecular Vision 2003; 9:410-9
42. Ahmed F, Brown KM, Stephan DA, Morrison JC, Johnson EC, Tomarev SI. Microarray analysis of changes in mRNA levels in the rat retina after experimental elevation of intraocular pressure. Invest Ophthalmol Vis Sci 2004; 45:1247-58.
43. Steele MR, Inman DM, Calkins DJ, Horner PJ, Vetter ML. Microarray analysis of retinal gene expression in the DBA/2J model of glaucoma. Invest Ophthalmol Vis Sci 2006; 47:977-85.
44. Sakaguchi H, Miyagi M, Darrow RM, Crabb JS, Hollyfield JG, Organisciak DT, Crabb JW. Intense light exposure changes the crystallin content in retina. Exp Eye Res 2003; 76:131-3.
45. Vazquez-Chona F, Song BK, Geisert EE Jr. Temporal changes in gene expression after injury in the rat retina. Invest Ophthalmol Vis Sci 2004; 45:2737-46.
46. Jones SE, Jomary C, Grist J, Thomas MR, Neal MJ. Expression of alphaB-crystallin in a mouse model of inherited retinal degeneration. Neuroreport 1998; 9:4161-5.
47. Farjo R, Kern TS, Andley UP, Swaroop A. Microarray analysis of mouse models of diabetic retinopathy reveals dramatic modulation of crystallin genes in the retina. ARVO Annual Meeting, 2003 May 4-9.